Journal of Luminescence 210 (2019) 435–443

Contents lists available at ScienceDirect

Journal of Luminescence

journal homepage: www.elsevier.com/locate/jlumin

An in-depth study of the Judd-Ofelt analysis, spectroscopic properties and energy transfer of Dy^{3+} in alumino-lithium-telluroborate glasses

Vu Phi Tuyen[a,b], Vu Xuan Quang[a], Phan Van Do[c,*], Luong Duy Thanh[c], Nguyen Xuan Ca[d], Vu Xuan Hoa[d], Le van Tuat[e], Le Anh Thi[a], Masayuki Nogami[a,g]

[a] Institute of Research and Development, Duy Tan University, Da Nang, 550000, Viet Nam
[b] National Institute of Information and Communications Strategy - MIC, Hanoi, Viet Nam
[c] Thuyloi University, 175 TaySon, Dong Da, Hanoi, Viet Nam
[d] Faculty of Physics and Technology, Thai Nguyen University of Science, Thainguyen, Viet Nam
[e] Hue University of Science, Nguyen Hue Street, Hue City, Viet Nam
[g] Toyota Physical and Chemical Research Institute, Japan

ARTICLE INFO

Keywords:
Alumino-lithium-telluroborate glasses
Judd-ofelt theory
Inokuti-hirayama model

ABSTRACT

Dy^{3+}-doped glasses with compositions of $(69\text{-}x)B_2O_3 + 10TeO_2 + 10Al_2O_3 + 10Li_2O + xDy_2O_3$ (x = 0.1; 0.5; 1.0 and 2.0 mol%) were prepared by a melt–quenching technique. An in-depth Judd-Ofelt analysis has been carried out to estimate the influence of the hypersensitive transitions (HST) of Dy^{3+} on the validity of the obtained intensity parameters Ω_λ (λ = 2, 4, 6). The thermalization effect of the three-levels system of $^6H_{13/2}$ (level 0), $^4F_{9/2}$ (level 1) and $^4I_{15/2}$ (level 2) was taken into account to evaluate its radiative transition probabilities, life times and energy levels. The obtained results were compared with the experimental data to estimate the validity of the Judd-Ofelt analysis. The Inokuti-Hirayama model was used to analyze the luminescence decay curves. The dipole-dipole interaction was shown to be the dominant mechanism in energy transfer process through cross-relaxation between Dy^{3+} ions. The possibility to produce the light with chromaticity coordinates in the white-light region by mixing intense blue (484 nm, $^4F_{9/2} \rightarrow {}^6H_{15/2}$) and yellow (575 nm, $^4F_{9/2} \rightarrow {}^6H_{13/2}$) emissions of the single Dy^{3+} doped alumino-lithium-telluroborate glass was observed and estimated.

1. Introduction

Spectroscopic studies of rare earth (RE) doped crystal and glass materials provide valuable information about the energy level structure and radiative properties of RE ions [1–10]. The information is the important key to develop new optical devices such as lasers, light converters, sensors, optical fibers, amplifiers and lighting. In last several decades, much attention has been paid for generation of white light in the different glasses and crystals by incorporating rare earth ions and other metal ions [1,3,4]. Advantages of these light sources are high luminous efficiency, high color rendering index, low cost, energy savings, small volume, environment friendliness and long lifetime span [1]. Trivalent dysprosium (Dy^{3+}) is one of the most abundant rare earth elements and is used extensively in optical devices such as lighting, infrared laser, fiber amplifier, solar cells, telecommunication and mid-infrared wavebands … [6–8]. Especially, Dy^{3+} ion has attracted considerable interest because it alone is capable of generating white light [6,9]. Dy^{3+} ions-doped crystals [10–13], glasses [6,7,14,15] and glass-ceramic [8] have been extensively studied due to its primary intense blue (484 nm, $^4F_{9/2} \rightarrow {}^6H_{15/2}$) and yellow (575 nm, $^4F_{9/2} \rightarrow {}^6H_{13/2}$) emissions. An appropriate combination of these blue and yellow luminescence bands leads to generation of white light in many different compounds [6,9,16]. Moreover, these Dy^{3+}-doped solid state systems can be easily excited by the commercial UV or blue LEDs because there is a spectral overlap between the excitation spectra of the Dy^{3+} ion and the LED's emission [6,24]. Additionally, due to the well established optical properties, simple energy structure and spectra of Dy^{3+} ions in the different host matrices, these ions are normally used as a spectroscopic probe for studying the local symmetry and bonding features of the RE^{3+} ions [8,16]. It is well-known that the degree of covalence between Dy^{3+} and O^{2-} ions is indicated by the yellow-to-blue ratio of Dy^{3+} emission which can be varied by changing the glass system, dysprosium ions concentration, heat-treatment conditions and chemical compositions of hosts [6,8,14–16].

It is noted that crystals doped with RE^{3+} ion are the optical materials with large emission cross section and high quantum efficiency

* Corresponding author.
E-mail address: phanvando@tlu.edu.vn (P. Van Do).

https://doi.org/10.1016/j.jlumin.2019.03.009
Received 3 November 2018; Received in revised form 3 March 2019; Accepted 4 March 2019
Available online 05 March 2019

[11–13,17]. Therefore, they have great application potential for laser, lighting and optical amplifier [11,12]. However, the fabrication and adjustment of components as well as sizes of crystal are very difficult due to the high demand of fabrication technology [13,17–20]. Moreover, the mechanical reliability and rare earth solubility of crystals are not high [17]. Compared with the crystalline materials, glasses are favorable host for RE ions because of their broad inhomogeneous band width, possibility of tuning the wavelength, large doping capability, simple preparation procedure, easy components adjusting, low production cost and high mechanical reliability and rare earth solubility [14–16,21–24]. Among the oxide glasses, borate based glasses have been studied widely due to their special physical properties like excellent heat stability and lower melting temperature in comparison with other glasses [21]. Tellurite based glasses possess encouraging properties like low melting points, slow crystallization rates, good thermal and chemical stability, low cut off phonon energy and high refractive index as well as nonlinear refractive index, which favors the spontaneous emission [22,23]. The pure borate based glasses possess high phonon energy in the order of 1300–1600 cm^{-1}, and the TeO_2 based glasses show the phonon energy in the order of 600–800 cm^{-1}. When the borate glasses are added with TeO_2, they can result in significant reduction in the phonon energy [24,25].

Because of the advantages of the tellurite glasses as well as the technological importance of Dy^{3+} ions, the Dy^{3+}-doped tellurite glasses have been recently studied by many authors [26–31]. However, there have been, to the best of our knowledge, only limited investigations on trivalent dysprosium ions doped in the boro-tellurite glass. In present research, we would like to focus our studies on the alumino-lithium-telluroborate (BTAL) glasses doped by Dy^{3+} ions. It should be noted that the B_2O_3 oxide usually plays both roles: the former and the modifier component in the B_2O_3-TeO_2 glasses [24]. With a relative high content of B_2O_3 (larger 30 mol %), the strong interaction between B_2O_3 and TeO_2 components will establish the special properties in structural of glasses [24,32]. According to the article [33], the pure B_2O_3 glass consists primarily of random network of boroxyl rings and [BO_3] triangles connected by B-O-B linkages. In alumino-lithium-telluroborate glass, Li_2O oxide plays a role in modifier component whereas TeO_2 oxide can act two roles including glass former at high content and network modifier at low concentration [9,24,33]. The addition of Li_2O can modify the rings in borate network through the transforing of [BO_3] to [BO_4] units [5,9,33,35,36]. These structure groups are linked by oxygen atoms [5]. Furthermore, the presence of Li^+ in glass decreases viscosity and melting points of the material by disrupting the glass network and creating non-bridging oxygens [9,33]. It is noted that TeO_2 is a heavy metal oxide so it has low phonon energy, high durability, large electronic polarizability and low crystal field strength [9,24,30,31]. The addition of TeO_2 to borate glass can reduce phonon energy and increase refractive index as well as transparency of material which cause the luminescence enhancement from excited states of RE^{3+} ions due to the reduce of nonradiative relaxation rates [9,24,31]. Additionally, when the modifier cations (Li^+ and Te^{4+}) replace the sites of B^{3+} ions in glass, the asymmetry of local structure increases because of the difference between ion radius of Li^+ or Te^{4+} ions and that of B^{3+} ion [9,33,34]. The distortion of local structure affects strongly the crystal-field environment around RE^{3+} ion leading to increase in radiative transition probability from the excited state to the ground state of RE^{3+} ion [34,37].

In this paper, we present an in-depth investigation of the spectroscopic and luminescence properties of Dy^{3+} in BTAL glasses by following the Judd-Ofelt (JO) theory [38,39] and other spectroscopic methods. The JO spectroscopic analysis is performed using the room temperature absorption spectrum of Dy^{3+} ions doped in the BTAL glasses. The specifically spectroscopic and luminescence properties are studied and compared to those of Dy^{3+} - doped in other glass hosts. The energy transfer process between Dy^{3+} ions in BTAL glass has been also discussed in detail.

2. Experiment

Alumino-lithium-telluroborate glasses doped with dysprosium (BTAL:Dy^{3+}) were prepared by following compositions:

BTAL01: $69.9B_2O_3 + 10TeO_2 + 10Al_2O_3 + 10Li_2O + 0.1Dy_2O_3$

BTAL05: $69.5B_2O_3 + 10TeO_2 + 10Al_2O_3 + 10Li_2O + 0.5Dy_2O_3$

BTAL10: $69B_2O_3 + 10TeO_2 + 10Al_2O_3 + 10Li_2O + 1Dy_2O_3$

BTAL20: $68B_2O_3 + 10TeO_2 + 10Al_2O_3 + 10Li_2O + 2Dy_2O_3$

The starting mixed powder was grinded in an agate mortar and melted in an electric furnace at 1040–1100 °C for 1 h in a cover platinum crucible. The liquids were poured into reheated copper plate and pressed with another copper plate so that the glassy samples in the form of discs were obtained. The obtained glass samples were subsequently annealed at 400 °C for 6 h, after that they were slowly cooled down to room temperature. This annealing process was made to avoid the undesirable thermal strain. For optical measurements, the glass samples were sliced and polished to get a uniform thickness of 2 mm.

Absorption spectra were carried out using Cary 5E (Varian Instruments, Sugar lane, Tex) in the wavelength region 200–2500 nm with a spectra resolution of 1.0 nm. The emission and excitation spectra were recorded in a Fluorog 3–22 (Horiba Jobin-Yvon) with 450 W Xelamp at room temperature. Refractive index for these glasses was measured by an Abbe's refractometer at sodium wavelength. Luminescence lifetime was measured using a Varian Cary Eclipse Fluorescence Spectrophotometer. All the measurements were performed at room temperature.

3. Result and discussion

3.1. Absorption spectra and bonding parameter

Absorption spectra of the Dy^{3+} -doped BTAL glass in two regions of wavelength 250–400 nm and 700–1400 nm are showed in Fig. 1. Fourteen absorption bands are observed in the absorption spectra of Dy^{3+} ions. They are assigned for the transitions between the levels in $4f^9$ electronic configuration from $^6H_{15/2}$ ground state to excited levels of Dy^{3+} ions [16,24,40,41]. The energy of these absorption transitions of Dy^{3+} ion in glass host is also compared with that of Dy^{3+}-diluted acid solution (aqua-ion) system [48] and is shown in Table 1. All peaks correspond to the wavelength positions to dysprosium manifolds. This result indicates the optical purity of the prepared samples. It is seen that, in the UV-region, the absorption of different electronic levels overlap and the assignments to each separated transition cannot be made easily due to the dense energy level scheme of Dy^{3+} ions. Besides, the absorption bands in the NIR wavelength range have stronger intensities because these transitions satisfy well the spin selection rule. Therefore, the absorption bands in the NIR region are used for JO analysis.

Nephelauxetic ratio (β) and bonding parameter (δ) are used to evaluate the nature of RE^{3+}- ligand bond in the any hosts. The nephelauxetic ratio is calculated by $\beta = \nu_c/\nu_a$, where ν_c and ν_a are energies of the corresponding transitions in the complex and in aqueous solution [13,17,24]. The bonding parameter is defined as $\delta = [(1 - \bar{\beta})/\bar{\beta}] \times 100$, where $\bar{\beta} = (\sum \beta)/n$ and n is the number of levels that are used to compute $\bar{\beta}$ values. The β and δ parameters of Dy^{3+} -doped BTAL glasses have been calculated and shown in Table 1.

The value of δ is negative for all samples. Thus, the Dy^{3+}-ligand bonding in BTAL:Dy^{3+} glasses are ionic bonding. This result is in good agreement with those published in Refs. [24,28,42–44] where the Dy^{3+} ions also exhibited ionic character in glasses.

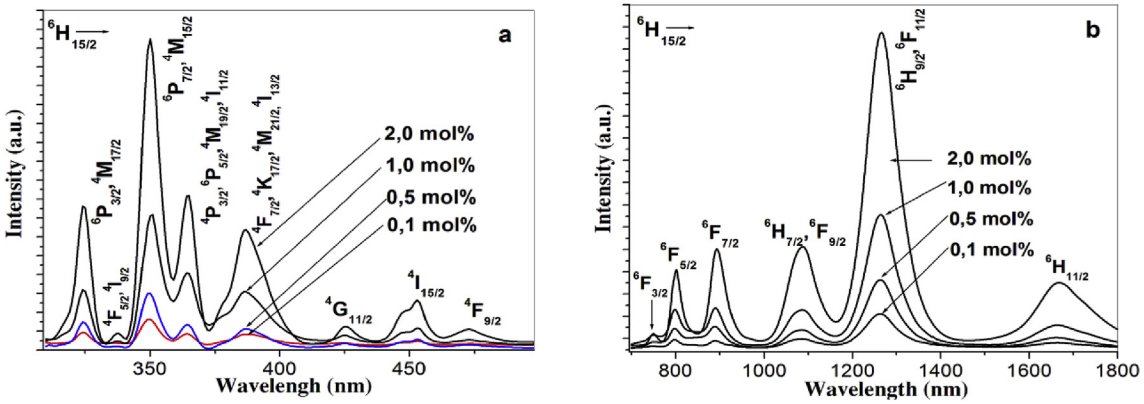

Fig. 1. Room temperature absorption of BTAL:Dy^{3+} glasses in UV–Vis (a) and near infrared (b) spectral regions.

3.2. The influence of the hypersensitive transitions on the Judd-Ofelt analysis

3.2.1. The JO fitting procedure

The Judd-Ofelt theory [38,39] was shown to be an effective method to characterize radiative transitions for RE^{3+}-doped solids. This theory defines a set of three intensity parameters, Ω_λ ($\lambda = 2, 4, 6$), that are sensitive to the environment of the rare-earth ions [45]. These parameters could be used to predict radiative properties of the rare earth ions in materials such as the radiative transition probability, radiative lifetime and branching ratios etc. (the radiative transition probability gives the likelihood of a spontaneous radiative emission event; the lifetime is the time that an ion remains in an exited state and branching ratios is a measure of fraction of photon flux). Those three parameters experimentally determined from absorption spectra and the refractive indices of the host matrix are used to predict the fluorescence intensities of the transitions.

According to the JO theory, the electric dipole oscillator strength of a transition from the ground state to an excited state is given by Refs. [13,17,24,41].

$$f_{cal} = \frac{8\pi^2 mc\nu}{3h(2J+1)} \times \frac{(n^2+2)^2}{9n} \sum_{\lambda=2,4,6} \Omega_\lambda \|U^{(\lambda)}\|^2 \quad (1)$$

where n is the refractive index of the material, J is the total angular momentum of the ground state, Ω_λ are the JO intensity parameters and $\|U^\lambda\|^2$ are the squared doubly reduced matrix of the unit tensor operator of the rank $\lambda = 2, 4, 6$, which are calculated from intermediate coupling approximation for a transition $|\psi J\rangle \rightarrow |\psi' J'\rangle$. These reduced matrix elements are nearly independent from host matrix as noticed from earlier studies [41,46].

On the other hand, the experimental oscillator strengths, f_{exp}, of the absorption bands are determined experimentally using the following formula [13,17,24].

$$f_{exp} = 4,318.10^{-9} \int \alpha(\nu) d\nu \quad (2)$$

where α is molar extinction coefficient at energy ν (cm^{-1}). The values of $\alpha(\nu)$can be calculated from absorbance A by using Lambert–Beer's law [13,15].

$$A = \alpha(\nu) cd \quad (3)$$

where c is concentration [dim: L^{-3} units: mol/l], d is the optical path length [dim: L; units: cm].

By equating the measured and calculated values of the oscillator strength ($f_{cal} = f_{exp}$) and solving the system of equations by the method of least squares, the JO intensities parameters Ω_λ ($\lambda = 2$, 4 and 6) have been evaluated numerically. To do this, we used the reduced matrix elements reported by Ref. [46] and the values of the refractive index was measured to be 1.562, 1.564, 1562 and 1.553 for the BTAL01, BTAL05, BTAL10 and BTAL20 samples, respectively. Overlap of the absorption bands (see Fig. 1) was considered in the analysis by taking the sum of the squared matrix elements over the inter-manifold transitions involved [6,24].

In this case, we can take advantage of the property that both the dipole strengths and the squared reduced matrix elements of overlapping transitions are additive. For the transitions overlap, it is necessary to integrate all the transitions contribution to one absorption band together. The corresponding reduced matrix elements have to be summed (for example, the additive technique were used for overlapped

Table 1
Energy transitions (ν) and bonding parameters (δ) of Dy^{3+} ions in BTAL glasses.

$^6H_{15/2}\rightarrow$	aquo	BTAL01	BTAL05	BTAL10	BTAL20
$^6H_{11/2}$	5850	6012	5988	5983	5983
$^6H_{9/2}+{}^6F_{11/2}$	7700	7917	7912	7907	7907
$^6H_{7/2}+{}^6F_{9/2}$	9100	9208	9203	9192	9189
$^6F_{7/2}$	11,000	11,223	11,234	11,213	11,207
$^6F_{5/2}$	12,400	12,519	12,534	12,518	12,496
$^6F_{3/2}$	13,250	13,408	13,355	13,378	13,366
$^4F_{9/2}$	21,100	21,097	21,112	21,103	21,118
$^4I_{15/2}$	22,100	21,918	21,932	21,930	22,939
$^4G_{11/2}$	23,400	23,584	23,504	23,492	23,485
$^4F_{7/2}+{}^4K_{17/2}+{}^4M_{21/2}+{}^4I_{13/2}{}^4F_{7/2}$	25,800	25,839	25,803	25,839	25,839
$^4P_{3/2}+{}^4P_{5/2}+{}^4M_{19/2}+{}^4I_{11/2}$	27,400	27,472	27,436	27,425	27,412
$^6P_{7/2}+{}^4M_{15/2}$	28,550	28,571	28,602	28,535	28,554
$^4F_{5/2}+{}^4I_{9/2}$	29,600	29,673	29,648	29,673	29,626
$^6P_{3/2}+{}^4M_{17/2}$	30,800	30,864	30,854	30,816	30,812
$\bar{\beta}$	–	1.00846	1.00761	1.00711	1.00681
δ	–	- 0.838	- 0.755	−0.706	−0.676

bands $^6H_{15/2} \rightarrow {}^6H_{7/2} + {}^6F_{9/2}$, $^6H_{15/2} \rightarrow {}^6H_{9/2} + {}^6F_{11/2}$ … in the JO analysis of this study) [6,17,24].

3.2.2. The influence of the hypersensitive transitions on the JO analysis

The absorption band centered around 7917 cm^{-1} is related to the $^6H_{15/2} \rightarrow {}^6H_{9/2} + {}^6F_{11/2}$ transition that is dominant in the absorption spectra of Dy^{3+}. This transition obeys selection rules of $\Delta S = 0$, $\Delta L = 2$, $\Delta J = 2$ and is so-called "hypersensitive transition-HST" in Dy^{3+} ions [28,31]. The intensity of HST is influenced strongly by the local environment around Dy^{3+} ions and has an effect on the magnitude of Ω_λ parameters [16,47]. The specific influence of the hypersensitive transitions on the results of JO fitting procedure for Dy^{3+} ions in tellurite and ZBLAN glasses was investigated and discussed for the first time by Hormadaly and Reisfeld [47]. From these studies, it could be seen that by excluding the HST from the fitted transitions, the intensity of the remaining bands and the lifetime of the excited states are better accounted by the JO model compared with that received by the including the HST in the fitted transitions. Unlike the reported findings of Hormadaly and Reisfeld, Vijaya et al. have shown that the calculated results are close to experimental data for zinc fluorophosphate by using the HST [16]. However, the influence of the HST on the JO fitting procedure does not play important role as stated by most of the published results on Dy^{3+} doped materials. In order to clarify the effect of HST in BTAL:Dy^{3+} glasses, two cases (with and without the $^6H_{15/2} \rightarrow {}^6H_{9/2} + {}^6F_{11/2}$ hypersensitive transition) are separately considered during the fitting procedure. Table 2 shows the experimental (f_{exp}) and calculated (f_{cal}) oscillator strengths of transitions in BTAL20 sample for both inclusion and exclusion of the HST. In Table 2, the root mean square deviation value RMS of 0.87×10^{-6} was calculated from the experimental and calculated oscillator strengths for the inclusion of the HST. This indicates a good fit between experimental and calculated results.

For the exclusion of the HST, the deviation value RMS = 0.99×10^{-6} was obtained by the same approach.

Table 3 presents both obtained sets of intensity parameters Ω_λ (with and without HST in the fitting procedure) for BTAL glasses with different concentration of Dy^{3+} ions. The values of Ω_λ are almost independent on the concentration of Dy^{3+} ions. The obtained values of Ω_λ parameters in Table 3 show that: i) if the errors were taken into account, both obtained sets of JO parameters Ω_λ for each sample show the nearly same values. ii) The HST included fitting procedures give the smaller error of JO parameters Ω_λ. iii) These smaller errors were originated from the decreased RMS deviations, which were found in all HST included fitting procedures. It could be understood that, by excluding the strongest absorption band correspond to $^6H_{15/2} \rightarrow {}^6H_{9/2} + {}^6F_{11/2}$transition, the HST omitted fitting procedures could increase the RMS deviation and increase the error of the JO analysis. In our case, included or excluded HST does not affect significantly the magnitude of Ω_λ parameters. On the other hand, until now, the physical disagreements concerning the use of the HST in the JO fitting procedures are not yet known. Therefore, the intensity parameters obtained by the HST-included fitting procedure is used for the further investigations on samples.

Table 3
The JO intensity parameters Ω_λ ($\times 10^{-20}$ cm^2) and RMS ($\times 10^{-6}$) deviations of the glass samples.

Samples		Ω_2	Ω_4	Ω_6	RMS
BTAL01	Included HST	13.41 ± 1.01	2.75 ± 0.57	4.59 ± 0.59	0.98
	Omitted HST	13.14 ± 5.42	2.72 ± 1.08	4.62 ± 0.76	1.46
BTAL05	Included HST	14.42 ± 0.98	3.72 ± 0.65	4.57 ± 0.58	1.07
	Omitted HST	14.28 ± 5.72	3.26 ± 0.94	4.57 ± 0.76	1.43
BTAL10	Included HST	14.41 ± 1.01	3.36 ± 0.62	4.48 ± 0.59	0.95
	Omitted HST	14.05 ± 6.24	3.40 ± 1.09	4.45 ± 0.77	1.36
BTAL20	Included HST	13.85 ± 0.76	4.25 ± 0.71	4.73 ± 0.41	0.87
	Omitted HST	15.26 ± 6.42	4.44 ± 0.96	4.50 ± 0.45	0.99

3.3. The emission, excitation spectra and radiative properties

3.3.1. Excitation spectra and energy level diagram of Dy^{3+} ions in BTAL glasses

Fig. 2 shows the excitation spectrum of the BTAL05 sample monitored at wavelength 575 nm corresponding to the $^4F_{9/2} \rightarrow {}^6H_{13/2}$ fluorescence transition. The excitation spectra of BTAL:Dy^{3+} glasses are similar to those observed in the other glasses doped with Dy^{3+} [15,27,44]. Nine excitation bands are observed and are assigned to transitions from the ground level $^6H_{15/2}$ to the excited states $^4F_{9/2}$, $^4I_{15/2}$, $^4G_{11/2}$, $^4I_{13/2}$, $^6P_{5/2}$, $^6P_{7/2}$, $^4F_{5/2}$, $^4M_{17/2}$ and $^4F_{3/2}$. Two strong excited bands at wavelength of 350 nm and 365 nm corresponding to the $^6H_{5/2} \rightarrow {}^6P_{7/2}$ and $^6H_{5/2} \rightarrow {}^6P_{5/2}$ transitions, respectively, are usually used for measurement of luminescence spectra.

3.3.2. The specific features of the $^4F_{9/2}$state

The energy level diagram of Dy^{3+} ions in BTAL is shown in Fig. 3. It can be seen that the $^4F_{9/2}$ level of Dy^{3+} ions shows the specific features. The small energy gaps between all levels lying above 21,000 cm^{-1} assure their efficient non-radiative relaxation leading to the strong population of the $^4F_{9/2}$ state. On the other hand, this state is separated from the next lower lying level $^6F_{1/2}$ by about 7200 cm^{-1} that is too large for the multiphonon relaxation. Therefore, the depopulation process of the $^4F_{9/2}$ state includes only the radiative transitions and

Table 2
The experimental (f_{exp}) and calculated (f_{cal}) oscillator strengths of transitions in BTAL20 sample.

Transition	Including HTS		Excluding HTS	
	f_{exp} ($\times 10^{-6}$)	f_{cal} ($\times 10^{-6}$)	f_{exp} ($\times 10^{-6}$)	f_{cal} ($\times 10^{-6}$)
$^6H_{5/2} \rightarrow {}^6H_{11/2}$	2.63	2.53	2.63	2.67
$^6H_{9/2} + {}^6F_{11/2}$	13.67	13.68	–	–
$^6H_{7/2} + {}^6F_{9/2}$	4.86	5.27	4.86	5.23
$^6F_{7/2}$	4.06	4.22	4.06	4.08
$^6F_{5/2}$	2.67	1.94	2.67	1.85
$^6F_{3/2}$	0.33	0.37	0.33	0.35
$^4F_{9/2}$	0.45	0.32	0.45	0.31
$^4I_{15/2}$	0.95	0.86	0.95	0.89
$^4G_{11/2}$	0.41	0.15	0.41	0.16
$^4F_{7/2} + {}^4K_{17/2} + {}^4M_{21/2} + {}^4I_{13/2}$	4.36	1.54	4.36	1.59
$^4P_{3/2} + {}^4P_{5/2} + {}^4M_{19/2} + {}^4I_{11/2}$	3.02	2.85	3.02	2.75
$^6P_{7/2} + {}^4M_{15/2}$	7.47	7.38	7.47	6.65
$^4F_{5/2} + {}^4I_{9/2}$	0.21	0.34	0.21	0.32
$^6P_{3/2} + {}^4M_{17/2}$	2.43	2.26	2.43	1.63
	RMS = 0.87×10^{-6}		RMS = 0.99×10^{-6}	

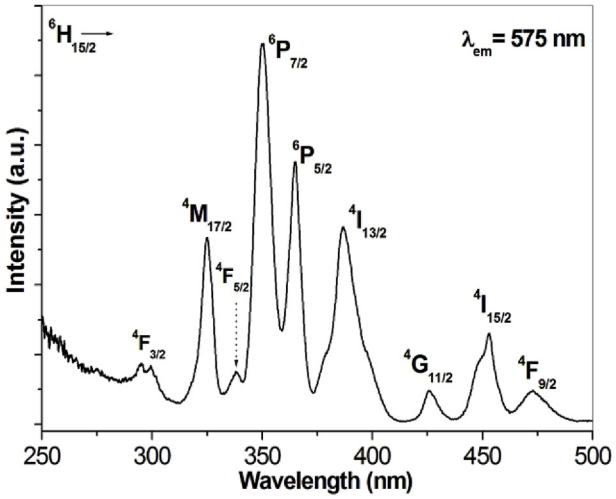

Fig. 2. The excitation spectrum monitored by wavelength 575 nm of BTAL05 sample.

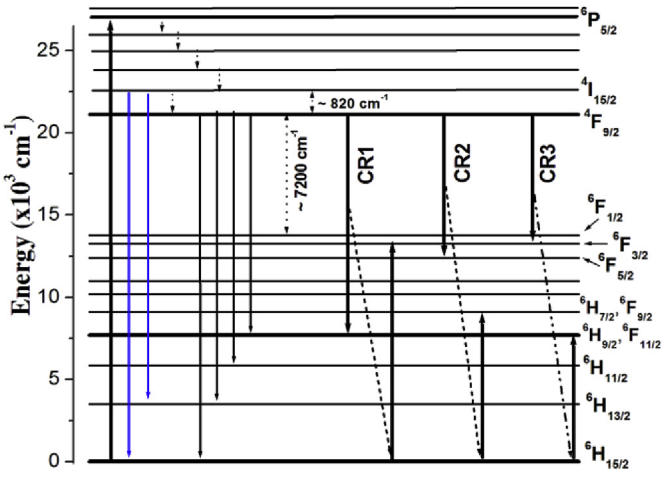

Fig. 3. Energy levels diagram and cross-relaxation (CR) channels for Dy^{3+} ions in BTAL glass.

relaxation by the non-radiative energy transfers. Beside that, the $^4F_{9/2}$ state locates very near the $^4I_{15/2}$ state (the energy separation between the $^4I_{15/2}$ and $^4F_{9/2}$ levels is found to be about 820 cm^{-1} in this case). Thus, the thermalization would be taken into consideration on the dynamics of these states.

3.3.3. Emission spectra

Fig. 4 illustrates the measured emission spectra using the 365 nm excitation wavelength of xenon lamp source. Four emission bands at 481, 575, 665 and 755 nm are attributed to transitions from $^4F_{9/2}$ to $^6H_{15/2}$, $^6H_{13/2}$, $^6H_{11/2}$ and $^6H_{9/2}+^6F_{11/2}$ states, respectively. Of the above-mentioned bands in the emission spectrum, the yellow (Y) band (575 nm) corresponding to the hypersensitive transition $^4F_{9/2} \rightarrow {}^6H_{13/2}$, ($\Delta L = 2$, $\Delta J = 2$) and the blue (B) band (481 nm) corresponding to the $^4F_{9/2} \rightarrow {}^6H_{15/2}$ transition are the dominant bands. Similar to the Eu^{3+} ions, the basic properties of trivalent Dy^{3+} in many host matrices are well understood. Consequently, these ions are extensively used as a spectroscopic probe for studying the structures and local symmetry of solid state materials [16,24].

The Y- band is hypersensitive and its intensity strongly depends on the host, in contrast to less sensitive B-band. Therefore the Y/B ratio is strongly changed with the glass compositions. The higher values of Y/B indicate the larger distortion of site symmetry and the degree of covalence between Dy^{3+} and oxygen ions. With this specific feature,

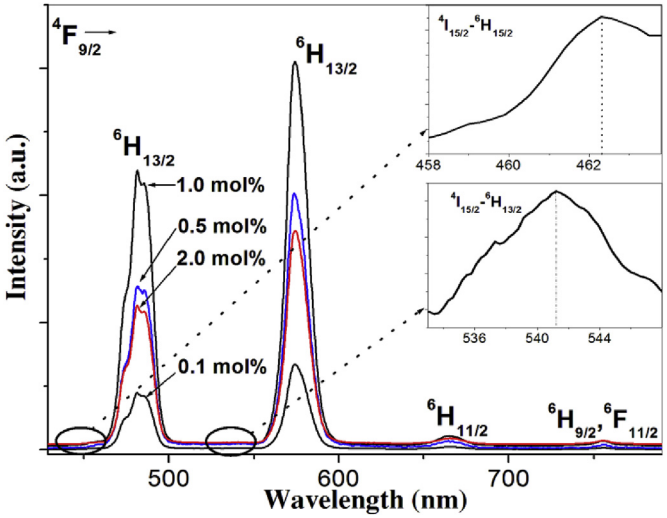

Fig. 4. The emission spectra of Dy^{3+} ions in BTAL glasses.

the Dy^{3+} ion is one of two best rare earth ions (another one is Eu^{3+} ion) used as the optical probe to study relation between glass composition, bonding nature and local symmetry in its surrounding. The Y/B ratios of the BTAL glass samples and some other glasses are calculated and presented in Table 7. It is seen that the Y/B ratios of BTAL:Dy^{3+} glasses are larger than unity for all samples. Thus, the yellow emission is dominant in BTAL:Dy^{3+} glasses. This shows that the environment around Dy^{3+} ions has the low symmetry without inversion center [8]. Besides, the values of Y/B in the BTAL:Dy^{3+} glasses are larger than that of other glasses [15,16,24,27]. This can be due to the higher asymmetry of the ligand and covalent of Dy^{3+}-ligand bond in BTAL:Dy^{3+} glasses [15,16,27].

3.3.4. The $^4I_{15/2}$ and $^4F_{9/2}$ levels

It is well-known that the energy gap between the levels $^4I_{15/2}$ and $^4F_{9/2}$ is about 700–800 cm^{-1} [15,16,41] corresponding to the energy of a typical phonon in the tellurite glasses [22,23]. In this case, two electron transition processes could happen simultaneously between these two levels: the electron could be transferred easily from $^4I_{15/2}$ level to $^4F_{9/2}$ level through the multiphonon transitions. On the other hand, the electron from the $^4F_{9/2}$ level could be transferred to the $^4I_{15/2}$ level by the thermal population process. The first process populates the $^4F_{9/2}$ level and contributes to the $^6H_{15/2} \rightarrow {}^4I_{15/2}$ excitation band. The second process is the origin of the emission processes corresponding to the $^4I_{15/2} \rightarrow {}^6H_J$ (J = 15/2, 13/2, 11/2 and 9/2) transitions. These emission bands can be observed by a zoom technique (see inset of Fig. 4) in our luminescence experiments.

The intensity ratios between the $^4I_{15/2} \rightarrow {}^6H_J$ and $^4F_{9/2} \rightarrow {}^6H_J$ emission bands could be evaluated quantitatively. According to the Boltzmann distribution, the transition probability of the electrons from the $^4F_{9/2}$ level to the $^4I_{15/2}$ level at the temperature T is given by Ref. [48]:

$$\frac{N_I}{N_F}(\%) = \frac{I_I}{I_F}(\%) = \exp\left\{-\frac{\Delta E}{kT}\right\} \times 100 \quad (4)$$

where N_I and N_F are ion numbers of Dy^{3+} ions in the $^4I_{15/2}$ and the $^4F_{9/2}$ levels, respectively, k is Boltzmann constant, ΔE term is the energy gap between the $^4I_{15/2}$ and $^4F_{9/2}$ levels ($\Delta E \approx 820\ cm^{-1}$). At room temperature, $kT = 201.6\ cm^{-1}$. I_I and I_F are the emission intensities of the $^4I_{15/2} \rightarrow {}^6H_{15/2}$ and $^4F_{9/2} \rightarrow {}^6H_{15/2}$ transitions, respectively. For the BTAL05 sample, we calculate $I_I/I_F \approx 1.72\%$ whereas the obtained result from emission spectrum is about 1.95%. Therefore the intensities of emission bands originated from $^4I_{15/2}$ level are much smaller than that from the $^4F_{9/2}$ level. All these emission bands can be observed in Fig. 4.

Table 4
Transition energies (ν), radiative transition probabilities (S_{ed}, S_{md}, A_R and A_T), radiative lifetime (τ_R) and branching ratios (β) for $^4I_{15/2}$ and $^4F_{9/2}$ excited levels of the BTAL01 sample.

$^4I_{15/2}\rightarrow$	ν(cm^{-1})	S_{ed} (× 10^{-40})	S_{md} (× 10^{-40})	A (s^{-1})	β_{cal} (%)	β_{exp} (%)
$^4F_{9/2}$	820	49	0	0.29	0.05	–
$^6F_{1/2}$	8243	0	0	0	0	–
$^6F_{3/2}$	8804	0.11	0	0.51	0.06	–
$^6F_{5/2}$	9609	0.04	0	0.24	0.03	–
$^6F_{7/2}$	11,041	0.05	1.74	0.88	0.10	–
$^6H_{5/2}$	11,852	0.03	0	0.36	0.04	–
$^6H_{7/2}$	12,915	0.18	0.77	2.94	0.35	–
$^6F_{9/2}$	12,998	1.67	0.69	24.72	2.92	–
$^6F_{11/2}$	14,321	3.17	0.10	62.11	7.32	–
$^6H_{9/2}$	14,350	0.71	7.18	17.91	2.11	–
$^6H_{11/2}$	16,229	1.99	1.36	57.72	6.80	–
$^6H_{13/2}$	18,580	2.85	0	122.73	14.35	–
$^6H_{15/2}$	22,100	7.77	0	558.98	65.91	–
$A_T(^4I_{15/2})$ = 848 s^{-1}, τ_R = 1.179 ms						
$^4F_{9/2}\rightarrow$	**ν(cm^{-1})**	**S_{ed} (× 10^{-40})**	**S_{md} (× 10^{-40})**	**A (s^{-1})**	**β_{cal} (%)**	**β_{exp} (%)**
$^6F_{1/2}$	7283	0.03	0	0.14	≈0	–
$^6F_{3/2}$	7845	0.02	0	0.12	≈0	–
$^6F_{5/2}$	8650	2.16	0	14.89	0.79	–
$^6F_{7/2}$	10,082	0.68	0.40	7.98	0.43	–
$^6H_{5/2}$	10,892	0.41	0	5.61	0.30	–
$^6H_{7/2}$	11,955	1.55	0.18	28.63	1.51	–
$^6F_{9/2}$	12,039	0.77	0.16	14.74	0.78	–
$^6F_{11/2}$	13,361	1.61	0.02	41.01	2.16	–
$^6H_{9/2}$	13,390	1.20	1.65	35.99	1.89	1.04
$^6H_{11/2}$	15,269	3.51	0.31	134.73	7.09	4.37
$^6H_{13/2}$	17,620	22.21	0	1297.06	68.20	55.66
$^6H_{15/2}$	21,140	2.83	0	320.40	16.85	38.93
$A_T(^4F_{9/2})$ = 1901 s^{-1}, τ_R = 0.526 ms						

Beside the well-known luminescence bands of Dy^{3+} ions corresponding to the $^4F_{9/2}\rightarrow{}^6H_{15/2}$ (481 nm), $^4F_{9/2}\rightarrow{}^6H_{13/2}$ (575 nm) transitions, two especially weak luminescence bands corresponding to the $^4I_{15/2}\rightarrow{}^6H_{15/2}$ (462.2 nm), $^4I_{15/2}\rightarrow{}^6H_{13/2}$ (541 nm) transitions, respectively, could be observed (in inset).

3.3.5. Radiative properties of Dy^{3+} ions

The obtained JO parameters Ω_λ obtained by HST-included fitting procedure (see Table 3) are used to predict the radiative properties of excited states of Dy^{3+} ion such as electric (S_{ed}) and magnetic (S_{md}) dipole line strengths, spontaneous transition probabilities (A_R), radiative lifetime (ι_R) and branching ratios (β_{cal}). The details of this theory were shown in previous reports [13,17,49]. Table 4 presents the predicted values of the radiative parameters: A_R, τ_R, β_{cal} and β_{exp} of the emission processes from the $^4I_{15/2}$ and $^4F_{9/2}$ levels of BTAL01 sample. The obtained results were calculated by using the HST included intensity parameters Ω_λ of the samples.

The lifetime (τ_R) of excited levels ($^4F_{9/2}$ and $^4I_{15/2}$) has been calculated and is shown in Table 4 for the BTAL01 sample. When the thermalization process of the $^4I_{15/2}$ and $^4F_{9/2}$ level pair is taken into consideration, their common lifetime is defined as [50–53]:

$$\tau = \left[\frac{16A_T(^4I_{15/2})\exp\left(-\frac{\Delta E}{kT}\right) + 10A_T(^4F_{9/2})}{16\exp\left(-\frac{\Delta E}{kT}\right) + 10}\right]^{-1} \quad (5)$$

with $A_T(^4I_{15/2})$ = 848 s^{-1}, $A_T(^4F_{9/2})$ = 1901 s^{-1}, $\Delta E(^4I_{15/2}\text{-}^4F_{9/2}) \approx 820\,cm^{-1}$, the common lifetime of two levels is found to be 0.545 ms and the common radiative transition rate $W_t = 1/\tau$ = 1834 s^{-1}.

The luminescence branching ratio characterizes the possibility of attaining stimulated emission from any specific transition. Therefore, that is a critical parameter to the laser designer [29,44]. Mahamuda et al. [44] and Vijaya et al. [16] reported that if the branching ratio of an emission transition is greater than 50%, this transition is potentiality for laser emission. For BTAL:Dy^{3+} glasses, the measured branching ratios of the $^4F_{9/2}\rightarrow{}^6H_{13/2}$ transition are 55.66, 54.96, 55.87 and 54.76% for BTAL01, BTAL05, BTAL10 and BTAL20 samples, respectively. So, the radiative parameters of this transition such as effective line width ($\Delta\lambda_{eff}$), stimulated emission cross-sections ($\sigma_{\lambda p}$), gain band width ($\sigma_{\lambda p} \times \Delta\lambda_{eff}$) and optical gain ($\sigma_{\lambda p} \times \tau_R$) have been calculated for all samples and are presented in Table 5. The results show that the radiative parameters do not vary significantly with the concentration of Dy^{3+} ions and they are much larger than those of some other glasses [16,27,28,43,44]. Thus, BTAL:Dy^{3+} glasses are found to be suitable for developing the yellow laser and fiber optic amplifier [6,8,15,29,44].

3.3.6. Evaluation of the validity of the JO analysis for Dy^{3+} ions in BTAL glasses

Table 4 shows that there is a significant deviation between calculated and experimental branching ratio in Dy^{3+} ions. This large discrepancy has been also found in other reports [13–16,27,44,54]. However, the validity of JO analysis for Dy^{3+} ions is not yet addressed. Below is our possible discussion for that.

It is seen that the emission bands at around 541 and 575 nm correspond to the $^4I_{15/2}\rightarrow{}^6H_{13/2}$ and $^4F_{9/2}\rightarrow{}^6H_{13/2}$ transitions, respectively, which are originated from the levels $^4I_{15/2}$ and $^4F_{9/2}$. At room temperature, the thermalization of these two levels occurs. Therefore, a

Table 5
Radiative parameters for $^4F_{9/2}\rightarrow{}^6H_{13/2}$ transition in Dy^{3+} ions-doped BTAL glasses.

Sample	β_{exp} (%)	$\Delta\lambda_{eff}$ (nm)	$\sigma(\lambda_p)$ (10^{-22} cm^2)	$\sigma \times \Delta\lambda$ (10^{-28} cm^3)	$\sigma \times \tau_R$(10^{-25} cm^2s)
BTAL01	55.66	15.83	50.2	81.1	27.42
BTAL05	54.96	17.24	48.4	83.5	24.78
BTAL10	55.87	16.56	52.5	87.8	25.67
BTAL20	54.76	16.63	51.1	84.9	24.77

simple three-levels system comprised of $^6H_{13/2}$ (level 0), $^4F_{9/2}$ (level 1) and $^4I_{15/2}$ (level 2) could be used to describe the thermalization of the $^4I_{15/2}$ state by the following relation [52,53,55]:

$$\frac{I(^4I_{15/2})}{I(^4F_{9/2})} = \frac{A_T(^4I_{15/2})}{A_T(^4F_{9/2})}\frac{g_2}{g_1}\frac{h\nu_2}{h\nu_1}\exp\left(-\frac{\Delta E}{kT}\right) \quad (6)$$

where $A_T(^4I_{15/2}) = 848\ s^{-1}$, $A_T(^4F_{9/2}) = 1901\ s^{-1}$ are the total spontaneous-emission rate, $h\nu_1 = 17{,}649\ cm^{-1}$, is the energy of the highest experimental stark level of luminescence band $^4F_{9/2} \rightarrow {}^6H_{13/2}$ and $h\nu_2 = 18{,}437\ cm^{-1}$ is the energy of the lowest experimental stark level of the luminescence band $^4I_{15/2} \rightarrow {}^6H_{13/2}$, $g_2 = 16$, $g_1 = 10$ are the degeneracies $(2J + 1)$ of the $^4F_{9/2}$ and $^4I_{15/2}$ levels, respectively. The I terms represent the experimental integrated intensity of a given transition at room temperature. The experimental value of the ratio $\frac{I(^4I_{15/2})}{I(^4F_{9/2})}$ is found to be 0,009. From the experimental values of emission spectra and the predicted total spontaneous transition rate of the JO analysis and using Eq. (6), the predicted energy gap ΔE is found to be 891 cm^{-1}. This predicted value is in good agreement with the energy separation of 820 cm^{-1} between two nearest stark levels of the $^4F_{9/2} \rightarrow {}^6H_{13/2}$ and $^4I_{15/2} \rightarrow {}^6H_{13/2}$ bands. The difference of about 8.7% beween these values could be explained by the inherent error about 15–20% of the JO parameters [45,52]. From this result, we conclude that the JO analysis performed in this study may be used to explain satisfactorily the experimental results. The difference between calculated and experimental branching ratio may be related to the non-radiative processes from $^4F_{9/2}$ level of Dy^{3+} ions in BTAL:Dy^{3+} glasses [16,54].

3.4. Luminescence decay curve analysis

The measured fluorescence decay curves at 575 nm corresponding to $^4F_{9/2} \rightarrow {}^6H_{13/2}$ transition for all samples are shown in Fig. 5. Experimental lifetimes (τ_{exp}) of samples have been determined by Refs. [16,17,56,57]:

$$\tau_{exp} = \frac{\int tI(t)dt}{\int I(t)dt} \quad (7)$$

The experimental lifetime of $^4F_{9/2}$ is found to be 0.515, 0.485, 0.378 and 0.226 ms for the BTAL01, BTAL05, BTAL10 and BTAL20 samples, respectively. It is seen that the experimental lifetime τ_{exp} is smaller than calculated lifetime τ_R. Additionally, the lifetime decreases with increasing concentration of Dy^{3+} ions. The observed results may be related to nonradiative processes including of multiphonon relaxation and energy transfer through cross-relaxation between Dy^{3+} ions. For

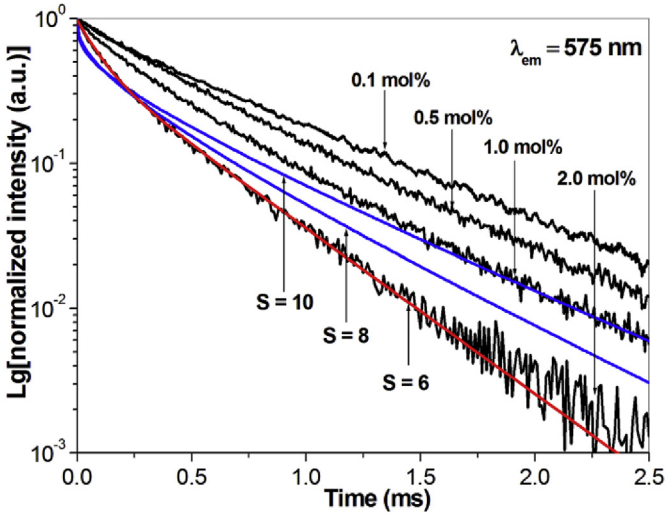

Fig. 5. Luminescence decay profiles of the $^4F_{9/2}$ level in Dy^{3+} ions doped BTAL glasses.

Dy^{3+} ions, the energy gap separating the emitting $^4F_{9/2}$ level from the next lower lying level $^6F_{1/2}$ (about 7200 cm^{-1}) is too large for the multiphonon relaxation. Therefore, the existence of some nonradiative energy transfer processes, such as the cross-relaxation process between the donor and acceptor in this material could be used to explain why the fluorescence lifetime is shorter than the radiative lifetime of the $^4F_{9/2}$ manifold. Some resonant and nearly resonant cross-relaxation channels in the Dy^{3+} doped BTAL are presented in Fig. 3: CR1: $(^4F_{9/2} \rightarrow {}^6H_{9/2}) \rightarrow (^6H_{15/2} \rightarrow {}^6F_{3/2})$; CR2: $(^4F_{9/2} \rightarrow {}^6H_{5/2}) \rightarrow (^6H_{15/2} \rightarrow {}^6F_{7/2})$ and CR3: $(^4F_{9/2} \rightarrow {}^6F_{3/2}) \rightarrow (^6H_{15/2} \rightarrow {}^6H_{9/2})$. The fluorescence quantum efficiency η is defined as the ratio of the number of photon emitted to the number photon absorbed. For this case, it is equal to the ratio of the experimental lifetime to the predicted lifetime for the $^4F_{9/2}$ level and given by Refs. [13,17,49]:

$$\eta(\%) = \frac{\tau_{exp}}{\tau_R} \times 100\% \quad (8)$$

The energy transfer rate through cross-relaxation is calculated by the formula [17,44]:

$$W_{ET} = \frac{1}{\tau_{exp}} - \frac{1}{\tau_R} \quad (9)$$

The calculated results for the η and W_{ET} are presented in Table 6. It is found that the quantum efficiency decreases whereas energy transfer rate increases with increasing concentration of Dy^{3+} ions. The difference between the relaxation and absorption energies for CR1, CR2 and CR3 channels are approximately 40, 400 and 50 cm^{-1}, respectively. Thus, the CR1 and CR3 channels can be considered to be resonant whereas the CR2 channel is assisted by phonon. In energy transfer processes assisted by phonons, the transfer probability is normally lower than that in the resonant situation [58]. Thus, the transfer probability through CR2 channel is smaller than those of CR1 and CR3 channels.

In the energy transfer process between RE^{3+} ions through cross-relaxation, the CR rate depends on the kind of modifier cations in glass. This CR rate is enhanced in glasses containing modifier cations with the small ionic radius (e.g. Li^+ ion) [34]. The reason is due to the dependence of energy transfer rate on the distance between RE^{3+} ions: the shorter the RE^{3+}-RE^{3+} distance is, the more the CR occurs [34]. The RE^{3+}-RE^{3+} distance in glasses consisting of the cations with small ionic radius is shorter than that with the large ionic radius [34].

As shown in Fig. 5, at the concentration of 0.1 mol% the fluorescence decay curve is nearly single exponential because the effect of the energy transfers is negligible at the very low Dy^{3+} concentration [16,28]. However, at higher concentration, the interaction between ions becomes stronger and energy can be transferred from an excited Dy^{3+} ion (donor) to a non excited Dy^{3+} ion (acceptor), leading to a nonexponential shape of the decay curve [16,17,28].

It is widely known that the Inokuti-Hirayama model [59] could be used to analyze the luminescence decay curve. Considering a non-exponential character of the decay curve, the time evolution of the Dy^{3+} luminescence intensity is fitted by formula [16,27,43,56]:

$$I(t) = I(0)\exp\left[-\frac{t}{\tau_0} - Q\left(\frac{t}{\tau_0}\right)^{3/S}\right] \quad (10)$$

where $I(t)$ is the luminescence intensity at t seconds after pulse excitation; $I(0)$ is the intensity of emission at $t = 0$; τ_0 is the intrinsic lifetime in the absence of energy transfer; S describes the interaction mechanism between ions: $S = 6$ for dipole-dipole (D-D), 8 for dipole-quadrupole (D-Q), and 10 for quadrupole-quadrupole (Q-Q) interaction; Q is the energy transfer parameter defined as:

$$Q = \frac{4\pi}{3}\Gamma\left(1 - \frac{3}{S}\right)N_A R_0^3 \quad (11)$$

$\Gamma(x)$ is Euler's gamma function, which is equal to 1.77 for D-D

Table 6
Energy transfer parameters between Dy^{3+} ions in BTAL glasses.

Sample	τ_R (ms)	τ_{exp} (ms)	η (%)	W_{ET} (s^{-1})	R (Å)	R_0 (Å)	Q	C_{DA} ($cm^6.s^{-1}$)
BTAL01	0.526	0.515	97.32	40.6	17.45	–	–	–
BTAL05	0.512	0.485	94.72	108.73	10.21	7.12	0.58	2.89×10^{-40}
BTAL10	0.499	0.378	75.75	641.5	8.06	7.46	1.35	3.91×10^{-40}
BTAL20	0.485	0.226	46.59	2362.9	6.42	7.76	3.03	4.93×10^{-40}

interaction, 1.43 for D-Q interaction and 1.30 for Q-Q interaction. N_A is the concentration of Dy^{3+}; R_0 is the critical transfer distance for which the energy transfer rate equals the spontaneous decay rate τ_0^{-1}. The fluorescence decay curve is fitted by using Eq. (10) considering Q as free parameters and τ_0 value is lifetime of BTAL01 sample (0.515 ms). The three possible transfer mechanisms were taken into consideration, and the good fitting was found for $S = 6$. This result indicates that the energy transfer induced by the electric dipole-dipole transfer mechanism plays the main role in this case. The D-D dominant interaction between Dy^{3+} ions has been also found in some hosts such as zinc fluorophosphate [16], titanium-tungstate tellurite [28] lead phosphate [43], zinc alumino lead borate [9] and bismuthate [60] glasses. In fact, the fluorescence and lifetime quenching of RE^{3+} in oxide glasses are not only related to the cross-relaxation mechanism between RE^{3+} ions but also to other energy transfer processes such as migration energy [58,61], energy transfer between RE^{3+} ions and the intrinsic defects [56,62] or the OH^- groups [54,63]. However, these processes are not taken into account in the IH model. Consequently, there is a deviation between the theoretical curve and the experiment data as shown in Fig. 5.

From the obtained values of energy transfer parameter Q and concentration of Dy^{3+} the critical transfer distance R_0 is found. The distance R between Dy^{3+}-Dy^{3+} ion can be calculated by formula: $R = (3/4\pi N_A)^{-1/3}$. The interaction parameter is calculated by: $C_{DA} = R_0^6 . \tau_0^{-1}$. The results are shown in Table 6. It is shown that the values of Q, R_0 and C_{DA} parameters increase with increasing the concentration of Dy^{3+} ions. The calculated results also indicate that the parameters of Q and C_{DA} are strongly dependent on Dy^{3+} ion concentration.

3.5. White light emission

It should be pointed out that the intensity ratio of yellow emission to blue emission (Y/B) should increase when the Ω_2 value increases [12,13,24,46], according to the expression:

$$\frac{Y}{B} \sim \frac{0.051\Omega_2 + 0.0172\Omega_4 + 0.0573\Omega_6}{0.0\Omega_2 + 0.0049\Omega_4 + 0.0303\Omega_6} \quad (12)$$

Consequently, it is influenced by site asymmetries and electro-negativities of the ligand ions [64–66]. This feature could be used to get a desired value of the Y/B ratio by changing the host composition.

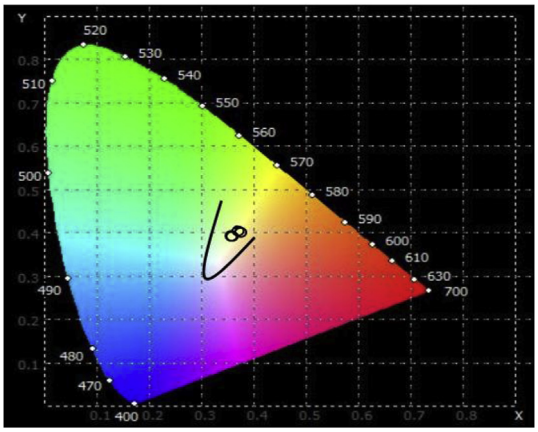

Fig. 6. CIE Chromatic coordinates diagram of Dy^{3+} ion in BTAL glasses.

The generation of white light of the system has been analyzed in the frame work of the chromaticity color coordinates [9,16]. The results are presented in Fig. 6 and Table 7. The result shows that the Y/B ratio depends weakly on the concentration of Dy^{3+} ions but strongly depend on the components of host. The changing of these ratios is originated from the changing in the environment of Dy^{3+} ions in the glasses as it involves a hypersensitive transition $^4F_{9/2} \rightarrow {}^6H_{13/2}$, ($\Delta L = 2$, $\Delta J = 2$). The Y/B ratio is very important for lighting technology. The line linking the yellow and blue wavelengths in the CIE 1931 chromaticity diagram usually passes through the white light region. Therefore, by adjusting to a suitable Y/B ratio, the chromaticity coordinates of the phosphors containing Dy^{3+} can be adjusted to the white light zone and these phosphors could be used suitably for the white-lighting.

The complicated dependence of the Y/B ratio and color coordination (x, y) values on the sample compositions in Table 7 could be explained by: i) the intensity of the hypersensitive Y band of Dy^{3+} ion is influenced very strongly by the symmetry and covalence degree in the surrounding environment around Dy^{3+} ions [64,65] and ii) the drastic dependence of the spectroscopic and structural features on the borate content of the boro-tellurite matrix, especially when the borate content

Table 7
The Y/B ratios, CIE coordination and CCTs calculated from the photoluminescence spectra with wavelength of 365 nm.

Sample	Y/B	x	y	CCT (K)	ref
$69.9B_2O_3$-$10TeO_2$-$10Al_2O$-$10Li_2O$-$0.1Dy_2O_3$	1.36	0.363	0.400	4604	Present
$69.5B_2O_3$-$10TeO_2$-$10Al_2O$-$10Li_2O$-$0.5Dy_2O_3$	1.37	0.362	0.400	4631	Present
$69B_2O_3$-$10TeO_2$-$10Al_2O$-$10Li_2O$-$1Dy_2O_3$	1.38	0.358	0.394	4721	Present
$68B_2O_3$-$10TeO_2$-$10Al_2O$-$10Li_2O$-$2Dy_2O_3$	1.38	0.358	0.394	4721	Present
$35B_2O_3$-$45TeO_2$-$9.5ZnO$-$10Na_2O$-$0.5Dy_2O_3$	1.32	0.350	0.400	–	[24]
$45B_2O_3$-$35TeO_2$-$9.5ZnO$-$10Na_2O$-$0.5Dy_2O_3$	1.51	0.330	0.420	–	[24]
$55B_2O_3$-$25TeO_2$-$9.5ZnO$-$10Na_2O$-$0.5Dy_2O_3$	1.02	0.310	0.360	–	[24]
$41P_2O_5$-$17K_2O$-$8Al_2O_3$-$23ZnF_2$-$10LiF$-$1Dy_2O_3$	0.77	0.320	0.365	5592	[16]
$15PbF_2$-$25WO_3$-$59TeO_2$-$1Dy_2O_3$	1.02	0.340	0.400	–	[27]
$26LiF$-$20PbO$-$10TeO_2$-$43H_3BO_3$-$1Dy_2O_3$	0.86	0.315	0.362	–	[31]
$10TeO_2$-$15CaO$-$5ZnO$-$10Nb_2O_5 59B_2O_3$-$1Dy_2O_3$	0.65	0.310	0.360	–	[15]
$50B_2O_3$-$10PbO$-$10Al_2O_3$-$10ZnO$-$19Li_2O$-$1Dy_2O_3$	1.301	0.345	0.385	5092	[9]
$50B_2O_3$-$10PbO$-$10Al_2O_3$-$10ZnO$-$19Na_2O$-$1Dy_2O_3$	1.286	0.346	0.383	5065	[9]
$50B_2O_3$-$10PbO$-$10Al_2O_3$-$10ZnO$-$19K_2O$-$1Dy_2O_3$	1.376	0.349	0.384	4964	[9]

is higher than 30% mol [24,35]. Nevertheless, it is clearly observed that the color coordinates of all BTAL:Dy^{3+} glass samples are found in the white region of the CIE diagram (Fig. 6). This result indicates that the present glasses could be suitable materials for generating white light.

The correlated color temperature (CCT) value is often used to analyze the type of light source [9,67]. The CCT value can be evaluated using the equation of McCamy [9,16,67]:

$$CCT = -449n^3 + 3525n^2 - 6823n + 5520.33 \quad (13)$$

where $n = (x - x_e)/(y - y_e)$ is the inverse slop line and ($x_e = 0.332$, $y_e = 0.186$) indicates the isotemperature lines epicenter.

The CCT values of the BTAL:Dy^{3+} glasses are presented in Table 7. It is noted that the CCT values are in region from 4604 to 4721 K corresponding to neutral white light. These results suggest that the prepared glasses are promising for practical applications such as displays and W-LEDs devices upon excitation by UV radiation.

4. Conclusion

It has been found that the HST included fitting procedures give a smaller root mean square deviation than the omitted HST. In consequence, the calculated JO parameters Ω_λ receive the smaller error. The thermalization effect of the three-levels system of $^6H_{13/2}$ (level 0), $^4F_{9/2}$ (level 1) and $^4I_{15/2}$ (level 2) is taken into account to predict the radiative transition probabilities, life time and energy gap of the Dy^{3+} ions. The comparison with experimental results indicates that the JO analysis is still valid for the Dy^{3+} ions. The quenching of the fluorescence lifetime is related to the energy transfer process through cross-relaxation between Dy^{3+} ions. Luminescence decay curves are analyzed by using the Inokuti-Hirayama model. Despite of the complicated relation between Y/B emission ratios of the Dy^{3+} and the host compositions, all the Dy^{3+} doped alumino-lithium-telluroborate glasses samples generate the visible emission spectra with chromaticity coordinates in the white light region under the excitation by 365 nm wavelength. Therefore, they have potential applications for white LED technology.

Acknowledgments

This research is funded by Vietnam National Foundation for Science and Technology Development (NAFOSTED) under grant number 103.03-2017.352.

Appendix A. Supplementary data

Supplementary data to this article can be found online at https://doi.org/10.1016/j.jlumin.2019.03.009.

References

[1] S. Ye, F. Xiao, Y.X. Pan, Y.Y. Ma, Q.Y. Zhang, Mater. Sci. Eng., R 71 (2010) 1.
[2] J. Xue, X. Wang, J.H. Jeong, X. Yan, Phys. Chem. Chem. Phys. 20 (2018) 11516.
[3] H. Dong, L.D. Sun, C.H. Yan, Chem. Soc. Rev. 44 (2015) 1608.
[4] H. Quo, R.F. Wei, X.Y. Liu, Opt. Lett. 37 (2012) 1670.
[5] Y. Yang, B. Chen, C. Wang, H. Zhong, L. Cheng, J. Sun, Y. Peng, X. Zhang, Opt. Lett. 36 (2008) 445.
[6] K.H.S. Shaaban, A.A. El-Maaref, M. Abdelawwad, Y.B. Saddeek, H. Wilke, H. Hillmer, J. Lumin. 196 (2018) 477.
[7] R. Wang, K. Yan, M. Zhang, X. Shen, S. Dai, X. Yang, Z. Yang, A. Yang, B. Zhang, B.L. Davies, Appl. Phys. Lett. 107 (2015) 161901.
[8] J. Guo, Q. Jiao, X. He, H. Guo, J. Tong, Z. Zhang, F. Jiang, G. Wang, Infrared Phys. Technol. 89 (2018) 115.
[9] G. Lakshminarayana, S.O. Baki, A. Lira, U. Caldiño, A.N. Meza-Rocha, I.V. Kityk, A.F. Abas, M.T. Alresheedi, M.A. Mahdi, J. Non-Cryst. Solids 481 (2018) 191.
[10] R.Y. Yang, H.L. Lai, J. Lumin. 145 (2014) 49.
[11] Z. Yang, Y. Liu, C. Liu, F. Yang, Q. Yu, X. Li, F. Lu, Ceram. Int. 39 (2013) 7279.
[12] S. Bigotta, M. Tonelli, E. Cavalli, A. Belleti, J. Lumin. 130 (2010) 13.
[13] P.V. Do, V.P. Tuyen, V.X. Quang, N.T. Thanh, V.T.T. Ha, H.V. Tuyen, N.M. Khaidukov, J. Marcazzo, Y.I. Lee, B.T. Huy, Opt. Mater. 35 (2013) 1636.
[14] J. Pisarska, R. Lisiecki, W.R. Romanowski, T. Goryczka, W.A. Pisarski, Chem. Phys. Lett. 489 (2010) 198.
[15] O. Ravi, C.M. Reddy, B.S. Reddy, B. Deva, P. Raju, Optic Commun. 312 (2014) 263.
[16] N. Vijaya, K. Upendra, C.K. Jayasankar, Spectrochim. Acta, Part A 113 (2013) 145.
[17] P.V. Do, V.P. Tuyen, V.X. Quang, N.M. Khaidukov, N.T. Thanh, B. Sengthong, B.T. Huy, J. Lumin. 179 (2016) 93.
[18] J.H. Zeng, J. Su, Z.H. Li, R.X. Yan, Y.D. Li, Adv. Mater. 17 (2005) 2119.
[19] X. Wang, Y. Bu, X. Yan, P. Cai, J. Wang, L. Qin, T.Q. Vu, H.J. Seo, Opt. Lett. 41 (2016) 5314.
[20] X. Wang, Y. Wang, Y. Bu, X. Yan, J. Wang, P. Cai, T.Q. Vu, H.J. Seo, Sci. Rep. 7 (2017) 43383.
[21] S.R. Anishia, M.T. Jose, O. Annalakshmi, V. Ramasamy, J. Lumin. 131 (2011) 2492.
[22] A.A. Ali, M.H. Shaaban, Physica B 403 (2008) 2461.
[23] V.P. Tuyen, T. Hayakawa, M. Nogai, J.R. Duclere, P. Thomas, J. Solid State Chem. 183 (2010) 2714.
[24] V.P. Tuyen, B. Sengthong, V.X. Quang, P.V. Do, H.V. Tuyen, L.X. Hung, N.T. Thanh, M. Nogami, T. Hayakawa, B.T. Huy, J. Lumin. 178 (2016) 27.
[25] J.C. McLaughlin, S.L. Tagg, J.W. Zwanziger, D.R. Haeffner, S.D. Shatri, J. Non-Cryst. Solids 274 (2000) 1.
[26] K. Damak, E.S. Yousef, C. Russel, R. Maalej, J. Quant. Spectrosc. Radiat. Transfer 134 (2014) 55.
[27] A.M. Babu, B.C. Jamalaiah, J.S. Kumar, T. Sasikala, L.R. Moorthy, J. Alloy. Comp. 509 (2011) 457.
[28] I. Jiothy, G. Upender, R. Kuladeep, D.N. Rao, Mater. Res. Bull. 50 (2014) 424.
[29] B.C. Jamalaiah, J. Phys. Condens. Matter 30 (2018) 335701.
[30] M.S.A. Mohd Saidi, R. Arifin, M.K. Roslan, R. Muhammad, W.N.W. Shamsuri, M. Abdullah, M.S. Shaharin, J. Alloy. Comp. 754 (2018) 171.
[31] S.A. Salem, B.C. Jamalajah, M. Jayasimhadri, A.S. Rao, K. Jang, L.R. Moorthi, J. Quant. Spectrosc. Radiat. Transfer 112 (2011) 78.
[32] S. Rada, M. Culea, E. Culea, J. Non-Cryst. Solids 354 (2008) 5491.
[33] Y.C. Ratnakaram, D.T. Naidu, A.V. Kumar, N.O. Gopal, Physica B 358 (2005) 296.
[34] N. Wada, K. Kojima, J. Lumin. 126 (2007) 53.
[35] T. Nishida, M. Yamada, H. Ide, Y. Takashima, J. Mater. Sci. Lett. 25 (1990) 3546.
[36] K. Maheshvaran, P.K. Veeran, K. Marimuthu, Solid State Sci. 17 (2013) 54.
[37] A.K. Parchur, R.S. Ningthoujam, RSC Adv. 2 (2012) 10859.
[38] B.R. Judd, Phys. Rev. 127 (1962) 750.
[39] G.S. Ofelt, J. Chem. Phys. 37 (1962) 511.
[40] V.M. Orera, P.J. Alonso, R. Cases, R. Alcala, Phys. Chem. Glasses 29 (1998) 59.
[41] W.T. Carnal, P.R. Fields, K. Rajnak, J. Chem. Phys. 49 (1968) 4424.
[42] P. Babu, C.K. Jayasanka, Opt. Mater. 15 (2000) 65.
[43] K. Linganna, ChS. Rao, C.K. Jayasankar, J. Quant. Spectrosc. Radiat. Transfer 118 (2013) 40–48.
[44] Sk Mahamuda, K. Swapna, P. Packiyaraj, A.S. Rao, G.V. Prakash, J. Lumin. 153 (2014) 382–392.
[45] K.A. Geschneidner, J.L. Eyhring, B.V. ElsevierScience, Handbook on the Physics and Chemistry of Rare Earths, Koerller-Walrand, K.Binneman, 1998, p. 101 Chapter 167.
[46] C.K. Jayasankar, E. Rulmini, Physca B 240 (1997) 273.
[47] J. Hormadaly, R. Reisfeld, J. Non-Cryst. Solids 30 (1979) 337.
[48] M. Kaczkan, Z. Boruc, S. Turczyński, M. Malinowski, J. Alloy. Comp. 612 (2011) 149.
[49] P.V. Do, V.P. Tuyen, V.X. Quang, N.T. Thanh, V.T.T. Ha, N.M. Khaidukov, Y. I Lee, B.T. Huy, J. Alloy. Comp. 520 (2012) 262.
[50] L.A. Risberg, W.H. Moss, Phys. Rev. 174 (1968) 429.
[51] G.D. Dzik, W.R. Romanowski, M.N. Palatnikov, N.V. Sidorov, V.T. Kalinnikov, J. Mol. Struct. 704 (2004) 139.
[52] B.T. Huy, B. Sengthong, P.V. Do, J.W. Chung, G.A. Kumar, V.X. Quang, V.D. Dao, Y.I. Lee, RSC Adv. 6 (2016) 92454.
[53] L.A. Riseberg, H.W. Moss, Phys. Rev. 174 (1968) 429.
[54] SdZ.A. Ahamed, C.M. Reddy, B.D.P. Raju, Opt. Mater. 35 (2013) 1385.
[55] M.D. Shinn, W.A. Sibley, M.G. Drexhage, R.N. Brown, Phys. Rev. B 27 (1983) 6635.
[56] P.V. Do, V.P. Tuyen, V.X. Quang, L.X. Hung, L.D. Thanh, T. Ngoc, N.V. Tam, B.T. Huy, Opt. Mater. 55 (2016) 62.
[57] P.V. Do, V.X. Quang, V.P. Tuyen, L.D. Thanh, N.M. Khaidukov, V.N. Makhov, N.T. Thanh, J. Lumin. 209 (2019) 340.
[58] V. Lavin, I.R. Martin, C.K. Jayasankar, Th Troster, Phys. Rev. B 66 (2002) 064207.
[59] M. Inokuti, F. Hirayama, J. Chem. Phys. 43 (1965) 1978.
[60] W.A. Pisarskia, J. Pisarska, R. Lisiecki, G.D. Dzik, W.R. Romanowski, Chem. Phys. Lett. 531 (2012) 114.
[61] R. Praveena, V. Venkatramu, P. Babu, C.K. Jayasankar, Th Troster, W. Sievers, G. Wortmann, J. Phys. Condens. Matter 21 (2009) 035108.
[62] V.K. Tikhomirov, A.B. Seddon, D. Furniss, M. Ferrari, J. Non-Cryst. Solids 326–327 (2003) 296.
[63] K. Maheshvaran, K. Linganna, K. Marimuthu, J. Lumin. 231 (2011) 2746.
[64] R. Peacock, The intensities of lanthanides f-f transitions, Rare Earths, Springer, Berlin Heidelbrg, 1975, pp. 83–122.
[65] H. Ebendorf-Heiderpriem, D. Ehrt, J. Non-Cryst. Solids 248 (1999) 247.
[66] P. Karthikeyan, R. Vijayakumar, K. Marimuthu, Phys. B Condens. Matter 521 (2017) 347.
[67] C.S. McCamy, Color Res. Appl. 17 (1992) 142.